Higher sensitivity towards light stress and ocean acidification in an Arctic sympagic compared to a pelagic diatom

Ane C. Kvernvik[1]* Sebastian D. Rokitta[2]*, Eva Leu[3], Lars Harms[2], Tove M. Gabrielsen[1], Björn Rost[2] and Clara J. M. Hoppe[2]

*These authors contributed equally to this study; [1]University Centre in Svalbard, Svalbard Science Centre, The Department of Arctic Biology, P.O. Box 156, N-9171 Longyearbyen, Norway; [2]Alfred-Wegener-Institut - Helmholtz-Zentrum für Polar- und Meeresforschung, Marine Biogeosciences, Am Handelshafen 12, 27570 Bremerhaven, Germany; [3]Arctic R&D, Akvaplan-Niva AS, CIENS, Gaustadalleen 21, 0349 Oslo, Norway

Authors for correspondence:

Ane Cecilie Kvernvik, Anek@unis.no

Sebastian D. Rokitta, Sebastian.Rokitta@awi.de

Word count

Total (excluding summary, references and legends):	6990
Summary	197
Introduction	754
Material & Methods	1722
Results	1961
Discussion	2474
Acknowledgements	72
Figures	4 (Figs 1-4 in color)
Tables	2
Supporting information	7 (Fig. S1; Table S1-S6)

Summary

- *Thalassiosira hyalina* and *Nitzschia frigida* are important members of Arctic pelagic and sympagic diatom communities. We investigated the effects of light stress (shift from 20 to 380 µmol photons m^{-2} s^{-1}, resembling upwelling or ice break-up) under contemporary and future pCO$_2$ (400 vs. 1000 µatm).

- The responses in growth, elemental composition, pigmentation and photophysiology were followed over 120 h and are discussed together with underlying gene expression patterns.

- Stress reaction and subsequent re-acclimation were efficiently facilitated by *T. hyalina*, which showed less pronounced and slower responses in photophysiology and elemental composition compared to *N. frigida*, and thrived under high-light after 120 h. In *N. frigida*, photochemical damage and oxidative stress appeared to overweigh cellular defenses, causing dysfunctional photophysiology and reduced growth. pCO$_2$ alone did not specifically influence gene expression, but amplified the transcriptomic reactions to light stress, indicating that pCO$_2$ affects metabolic equilibria rather than sensitive genes.

- Large differences in acclimation capacities towards high-light and high pCO$_2$ between *T. hyalina* and *N. frigida* indicate species-specific mechanisms in coping with the two stressors, possibly due to adaption to their respective ecological niches. This could potentially alter the balance between sympagic vs. pelagic primary production in a future Arctic.

Introduction

The Arctic ocean is changing fast in many respects, amongst which sea ice cover and pCO_2 stand out as being those changing most rapidly (IPCC, 2014). Irradiance levels in the upper mixed layers are expected to increase due to increased thermal stratification, declining snow cover, earlier melt onset accompanied by formation of melt ponds, and reduced summer sea-ice extent (Screen & Simmonds, 2010; Nicolaus *et al.*, 2012; Tremblay *et al.*, 2015). In addition, ocean acidification (OA) is most pronounced in the Arctic because CO_2 solubility increases at low temperatures, and the low total alkalinity makes the system sensitive to anthropogenic CO_2 loading (Yamamoto-Kawai *et al.*, 2009; AMAP, 2013). These two factors, i.e. irradiance regimes and pCO_2 levels, may not only affect the physiological performance, but also competitiveness and nutritional value of microalgae (Rost *et al.*, 2008; Kroeker *et al.*, 2013; Gao & Campbell, 2014; McMinn, 2017).

In order to cope with instantaneous light stress, diatoms utilize diverse mechanisms involving short- and long-term physiological changes. Short-term changes involve increased non-photochemical quenching (NPQ) of excitation energy, facilitated by the de- and re-epoxidation of the xanthophylls diadinoxanthin (DD) and diatoxanthin (DT). These pigments thermally dissipate excess excitation energy (Lavaud & Goss, 2014) and decrease overall stress derived from electron pressure and reactive oxygen species. Furthermore, algae decrease light-harvesting by increasing intracellular self-shading ('package effect') and by detaching antennae from photosystems (Giovagnetti & Ruban, 2017). Over longer time scales, diatoms alter pigment composition, typically increasing pigments related to photoprotection while decreasing those related to light harvesting (Brunet *et al.*, 2011). Studies have shown, however, that responses to changing light intensities can be modulated by high pCO_2 (Rost *et al.*, 2006; Li & Campbell, 2013; Hoppe *et al.*, 2015), which is often attributed to carbon-concentration mechanisms (CCMs) that elevate CO_2 around RubisCO under current, potentially limiting conditions (Giordano *et al.*, 2005): Since CCMs are energetically expensive (Hopkinson *et al.*, 2011), an increased diffusive CO_2 supply might lower its operational cost with corresponding energetic benefits (Trimborn *et al.*, 2009). However, other studies indicated that the sensitivity of diatoms to high-light stress increases under OA (Gao *et al.*, 2012; Hoppe *et al.*, 2015). These divergent results emphasize large inter- and intraspecific differences in CO_2 sensitivities (Rost *et al.*, 2008; McCarthy *et al.*, 2012). Hence, major alterations in bloom timing and the composition of algal assemblages are expected as a result of these ongoing changes. One of the major open questions is how the relative importance of primary production derived from pelagic

phytoplankton vs. sympagic, i.e. sea-ice associated microalgae will develop in the changing Arctic environment.

Both, the pelagic and sympagic ecosystems host diverse and distinct microalgal communities, which, due to the contrasting physico-chemical environments, exhibit specific adaptations to their respective habitats (Poulin *et al.*, 2011). Arctic phytoplankton communities are typically exposed to strong and rapid fluctuations in light regimes due to wind-driven overturning (MacIntyre *et al.*, 2000) and attenuation by riverine as well as glacial freshwater input. Yet, the regimes of temperature, salinity and carbonate chemistry are comparably stable. Hence, we hypothesized that pelagic algae are highly resilient towards photophysiological stress, while being responsive to OA. Within sea-ice, light intensities are extremely low, and fluctuations therein are small and typically slower (Hill *et al.*, 2018). However, sympagic ice-algal communities need to tolerate sub-zero temperatures, sustain net growth under such low irradiances (Hancke *et al.*, 2018), tolerate high salinities and extremely variable nutrient levels as well as distorted carbonate chemistry (Weeks & Ackley, 1986; McMinn *et al.*, 2014; Hill *et al.*, 2018). Despite the extreme physico-chemical properties of this habitat, ice-algae are widespread and often thrive remarkably (Aletsee & Jahnke, 1992). Hence, we hypothesized that ice algae can cope less well with instantaneous light stress, but exhibit high physiological plasticity to changing pH/CO_2 regimes under OA.

To investigate the responses of pelagic and sympagic diatoms, the common species *Thalassiosira hyalina* (Hegseth & Sundfjord, 2008) and *Nitzschia frigida* (Syvertsen, 1991; Leu *et al.*, 2015) were acclimated to low-light (20 µmol photons m^{-2} s^{-1}) and then exposed to a high-light scenario (380 µmol photons m^2 s^1) that resembled upwelling, ice break-up or melt-pond formation (Light *et al.*, 2015; Alou-Font *et al.*, 2016). This was done under contemporary and future pCO$_2$ (400 vs. 1000 µatm), so that the effects of high-light and OA can be investigated in isolation and combination. We followed the phenomenological and physiological reactions over a time course of several days and assessed the accompanying gene expression patterns to explore the underlying mechanisms that determine these species´ performance in a changing Arctic.

Materials and methods

Culture conditions and experimental setup

Dilute batch cultures of *Thalassiosira hyalina* (Grunow) Gran 1897 and *Nitzschia frigida* Grunow 1880 were grown in 1 L borosilicate bottles in 0.2 µm sterile-filtered Arctic seawater enriched with trace metals and vitamins according to f/2 media (Guillard & Ryther, 1962). Nitrate, phosphate and silicate were added in concentrations of 100, 25 and 60 µmol l^{-1}, respectively. Cultures were diluted every 2-5 days to exclude self-shading, nutrient limitation and changes in carbonate chemistry. Cells were grown under constant low-light (LL; ~20 µmol photons m^{-1} s^{-1}), provided by daylight lamps (Biolux T8, 6500K; Osram, München, Germany) and at two different CO_2 partial pressures (pCO_2; 400 vs. 1000 µatm). Cultures were acclimated to these conditions for >8 generations, before cells were exposed to high-light (HL; ~380 µmol photons m^{-2} s^{-1}). Irradiance was measured in cell-free culture bottles using a ULM-500 data logger (Li-Cor, Lincoln, NE, USA) equipped with a 4π sensor (Walz, Effeltrich, Germany). Bottles were placed in temperature-stabilized aquaria (2.3 ± 0.3 ^oC and 2.8 ± 0.4 ^oC for LL and HL, respectively). After the cells were exposed to HL, the immediate and the acclimation responses (after 5-7 days) were measured for each species.

Carbonate chemistry

Target pCO_2 was established by aerating the bottles with humidified air containing 400 and 1000 µatm CO_2, respectively, delivered through 0.2 µm sterile filters (Midisart 2000; Sartorius Stedim, Göttingen, Germany). Gas mixtures were generated by a gas mixing system as described in (Hoppe *et al.*, 2015). Stability of carbonate chemistry was ensured by daily pH measurements (NBS scale; Aquatrode plus Pt1000; Metrohm, Herisau, Switzerland). Samples of total alkalinity (TA) and dissolved inorganic carbon (DIC) were taken from each replicate as well as cell-free control bottles. TA samples were filtered (GF/F; Whatman, Maidstone, UK) and stored at ~4 ^oC until analysis. TA was measured by titration (Dickson, 1981) using a TitroLine burette (Schott Instruments, Mainz, Germany). DIC samples were filtered (0.2 µm cellulose-acetate syringe filters; Sartorius Stedim Biotech, Göttingen, Germany) and stored head-space free in 5 mL gas-tight borosilicate bottles at ~4 ^oC. DIC was determined using a QuaAAtro autoanalyzer (Seal Analytical, Norderstedt, Germany) following the method of Stoll et al. (2001). The carbonate system was calculated from DIC, pH, salinity, temperature, phosphate and silicate using CO_2SYS (Pierrot *et al.*, 2006; Table 1).

Growth, size and production rates

Cell concentrations were determined daily using a Multisizer III (Beckman-Coulter, Brea, CA, USA). To disrupt *N. frigida* chains, the cultures were shaken at 1500 rpm for 15 s (Precellys Evolution; Bertin, Bretinneux, France). Microscopy (Axio Observer.D1; Zeiss, Oberkochen, Germany) showed only single, intact cells after shaking. Specific growth rates were calculated by exponentially fitting the cell numbers over several days. Size was determined via light microscopy and Coulter Counter. For POC and PON quotas, cells were filtered onto precombusted (15 h, 500 °C) glass fiber filters (GF/F; Whatman, Maidstone, UK) and stored at -20 °C until further processing. Filters were soaked with 200 µl 0.2 mol l^{-1} HCl to remove residual inorganic carbon before measurements (EuroVector EA, EuroVector, Milano, Italy).

Pigment composition

Samples were collected on GF/F filters (Whatman, Maidstone, UK), flash-frozen in liquid nitrogen and stored at -80 °C until analysis. Filters were extracted for 24 h in a Teflon-lined tube with 1.6 ml 95% methanol, and then re-filtered through 0.45 µm filters (Millipore, Billerica, MA, USA), before the final extract was submitted to HPLC analysis. Pigment analyses followed Rodriguez *et al.* (2006) using a HP1100 HPLC system (Hewlett-Packard, Ramsey, MN, USA). The identification of pigments was based on retention times, pigment spectra obtained with diode array OD detector and commercially available pigment standards (Rodriguez *et al.*, 2006).

Chlorophyll a variable fluorescence

Chlorophyll (Chl) *a* variable fluorescence was measured using a Fast Ocean FRR fluorometer combined with a FastAct system (Chelsea Technologies, West Molesey, UK). Fluorescence-based photosynthesis measurements were conducted in triplicates after acclimation to LL and throughout the time course of HL exposure. Constant water pumping from the aquaria through the FastAct chamber prevented thermal change during measurements. Details on assay settings are given in Supporting Information (SI) table S1. To record photosynthesis versus irradiance (PE) curves, the FastAct provided 10 x 3 min levels of white PAR ranging from 0 to 1507 µmol photons m^{-2} s^{-1}. Following these actinic light periods, minimum (F_0') and maximum (F_m') fluorescence in light acclimated cells was determined and electron transfer rates (ETR, [mol e^{-} (mol RCII)$^{-1}$ s^{-1}]) of PSII were calculated (Eq. 1):

$$ETR = \frac{F_m{'} - F_0{'}}{F_m{'}} \cdot E_{PAR} \tag{1}$$

The calculated ETRs were plotted against actinic irradiance to generate PE curves, from which the light utilization coefficient (α) and the maximum photosynthetic rate (ETR_{max}) were derived by non-linear regression using the model of Eilers & Peeters (1988). The light acclimation index E_k was then calculated as ETR_{max}/α. Non-photochemical quenching of Chl$a$ fluorescence (NPQ) was measured in dark acclimated cells using the normalized Stern-Volmer coefficient (Oxborough *et al.*, 2012):

$$NPQ = \frac{F{'}_q}{F{'}_v} - 1 = \frac{F{'}_0}{F{'}_v} \tag{2}$$

Statistical analysis

All data presented are means of three or four replicates ± 1 SD. To test whether HL exposure significantly affected the algal photophysiology (F_v/F_m, σ_{PSII}, NPQ, α, ETR and E_k) or pigment content at different time points, one-way repeated measures (RM) ANOVA with subsequent normal distribution (Shapiro-Wilk) and *post-hoc* tests (Bonferroni t-test) were performed (SI Table S2). Two-way ANOVA with *post-hoc* tests (Holm-Sidak) were used to evaluate responses in POC and PON quotas, POC production, size fractions and growth rates, as well as the responses to high and low pCO_2 in LL and HL acclimated cells (SI Table S3). Statistical analyses were performed using the program SigmaPlot (SysStat Software, San Jose, CA, USA). Responses were deemed significant when the p-values were ≤0.05.

Differential gene expression analyses

In brief, cultures were concentrated by filtration and centrifugation, and flash frozen in liquid nitrogen. Total RNA was extracted after bead lysis of cells and on-column digestion of genomic DNA using the RNEasy Mini Kit (Macherey Nagel, Düren, Germany). Integrity and concentration of total RNA were verified using RNA6000 Lab Chips (Agilent, Waldbronn, Germany). 1 µg of RNA was used for cDNA library preparation (TruSeq HT paired end kit, Illumina, San Diego, California, USA) and the success of library preparation was verified with a LabChip GX electrophoresis (Perkin Elmer, Rodgau, Germany). Sequencing was performed in a High Output FlowCell V2 (Illumina, San Diego, California, USA) using a NextSeq 500 sequencer (Illumina, San Diego, California, USA). The run yielded ~950 million reads with an average read length of 136±8 basepairs. Trimmed raw data was made accessible at www.ebi.ac.uk under accession number E-MTAB-6999. Quality checks were performed with

FastQC (Andrew, 2010), showing that in <7% of the runs, the sequencing yielded low numbers of reads. Because replication was high enough, these samples were excluded from further analyses to avoid biases in relative quantification. Therefore, in two treatments, the replicate number was n=2. The tool bbduk.sh from the BBtools suite, version 36.38 (Bushnell, 2015) was used to remove sequences of adapters (parameters: ktrim=r, k=23, mink=11, hdist=1, tpe, tbo) and the Illumina spike-in 'PhiX' (parameters: k-mer size of 31 and an hdist of 1). Remaining rRNA sequences were identified using SortMeRNA version 2.1 (Kopylova *et al.*, 2012) and removed. A final quality trimming was performed with bbduk.sh using Q10 as minimum quality and 36 bases as the minimum length.

Due to lacking genomic databases for the two species, reference transcriptomes were generated. For this, all obtained sequences were normalized using bbnorm.sh (Bushnell, 2015) and de-novo assembled into transcripts using Trinity (Grabherr *et al.*, 2011), yielding 43,554 or 52,411 putative transcripts for *T. hyalina* and *N. frigida*, respectively (SI Table S5).

For differential gene expression (DGE) analyses, the obtained reads were processed using the software Genomics Workbench 10 (CLC Biosciences, Aarhus, Denmark). Reads were aligned to the transcripts and total read counts were normalized to intra-sample sequencing depth, yielding the *reads per kilobase per million mapped nucleotides* (RPKM; Mortazavi *et al.*, 2008). To account for different sequencing depths between samples, an additional per-sample library size normalization was implemented into the procedure, using the weighted trimmed mean of the log expression ratios (i.e. TMM-Normalization; Robinson & Oshlack, 2010).

To test for statistically significant DGE, the raw count data were evaluated by a separate generalized linear model, under the assumption that the expression follows a negative binomial distribution (Robinson *et al.*, 2010). Wald-tests were used to independently test for effects between the initial (0 h) and later time points (2, 24 and 120 h), under the precaution that pCO_2 might influence the data. Lastly, the GLM-derived significance estimates of DGE patterns were corrected for the statistical false discovery rates (FDR; Benjamini & Hochberg, 1995).

The dataset consisting of 43,554 or 52,411 transcripts and their expression patterns for *T. hyalina* and *N. frigida* was then reduced to isolate relevant DGE patterns and to yield a manageable size. To this end, transcripts were extracted that exhibited significant regulation (judged by an FDR-corrected p-value ≤0.05) with RPKM-based fold-change values ≥2.5 between the initial (0 h) and the first time point (2 h) in any of the pCO_2 levels. In addition, we extracted transcripts that had an RPKM-based fold-change value of ≥2.5 (based on mean

expression values of time points with non-overlapping standard deviations) between 2 h and 24 h in any of the pCO_2 levels, because physiological data indicated re-acclimation between these time points. Lastly, transcripts were extracted, that were highly expressed throughout the datasets, i.e. having mean RPKM expression levels ≥150 across both pCO_2 levels, which is about twice the average expression value of all genes in the species-specific datasets. These extracted transcripts (9,084 and 9,976 for *T. hyalina* and *N. frigida*, respectively) were then annotated using blastx, from the NCBI BLAST+ suite, version 2.5 with standard settings (Altschul *et al.*, 1990) and the NCBI RefSeq database (October 2017). The two best hits for every transcript were concatenated to the expression data, yielding DGE datasets of 5,954 and 6,143 transcripts of interest including their best- and second-best annotation (SI Table S6).

To assess possible OA modulation of the observed HL-responses, datasets were first examined towards transcripts that experienced a synonymous unidirectional regulation in both pCO_2 levels, i.e. transcripts that experienced either a HL-dependent up- or downregulation throughout the time course. For those transcripts that reacted synonymously to the HL-treatment, the pCO_2-related intensity change of the HL-response in every time step was calculated by dividing the respective fold-changes from the time course.

Results

Results of the HL-exposure time course are reported separately for *Thalassiosira hyalina* and *Nitzschia frigida* by comparing parameters between different time-points in cells grown at 400 µatm. After that, the effect of pCO_2 on the HL-response in both species is described.

HL-responses in T. hyalina

During the first 12 h of HL-exposure, the maximum dark-acclimated PSII quantum yield (F_v/F_m, Fig. 1a) decreased in *T. hyalina* from initially 0.60 ± 0.01 in LL to 0.32 ± 0.02. Henceforth, F_v/F_m increased again and, after 72 h, stabilized at a significantly lower level compared to LL (0.41 ± 0.03, SI Table S2). The absorption cross section of PSII (σ_{PSII}) increased rapidly and significantly during the first 15 min of HL-exposure (from 3.4 ± 0.1 to 3.9 ± 0.1 nm^2 PSII^{-1}), followed by a gradual decrease over the next 48 h, after which it reached a minimum at 2.5 ± 0.1 and more or less stabilized at this level until the end of the time course (Fig. 1b, SI Table S2). The capacity for non-photochemical quenching (NPQ) increased from 0.6 ± 0.0 to 2.2 ± 0.2 after 12 h in HL. Between 12 and 24 h, NPQ rose to the maximum level observed (4.5 ± 1.6), before decreasing and stabilizing at 1.4 ± 0.1 until the end of the time

course (Fig. 1c, SI Table S2). The light utilization coefficient α (Fig. 1d) was halved in *T. hyalina* after 12 h of HL-exposure, from initially 0.88 ± 0.06 to 0.38 ± 0.02. After 24 h, α reached minimal values (0.22 ± 0.05), then increased slightly, and stabilized at ~0.45 ± 0.06, by end of the time course (SI Table S2). Electron transport rates (ETR) were ~70 ± 6 mol e^- (mol RCII)$^{-1}$ s^{-1} over the first 12 hours of HL-exposure (Fig. 1e). At 24 h, they dropped rapidly and significantly to 42.8 ± 10.3, before they increased to 102.5 ± 5.9 mol e^- (mol RCII)$^{-1}$ s^{-1} in the course of re-acclimation (SI Table S2). The light acclimation index (E_k) increased from ~70 µmol photons m^{-2} s^{-1} in LL acclimated cells to ~230 µmol photons m^{-2} s^{-1} after ~48 h (Fig. 1f, SI Table S2). The cellular quotas of light harvesting pigments (Chl*a*, fucoxanthin or Chl*c* 1+2) in *T. hyalina* did not change significantly in response to the HL-exposure (Fig. 2a, SI Table S2). However, when normalized to POC, a significant reduction of 50% in response to HL became evident (Table 2, SI Table S3). The cumulative cellular quota of photoprotective pigments (diadinoxanthin + diatoxanthin, DD+DT) was significantly elevated after 24 h of HL-exposure, but decreased again to values similar to those found under LL by the end of the time course (24.8 ± 6.6 fg cell^{-1}, Fig. 2b, SI Table S2). *T. hyalina´s* growth rates, POC and PON quotas, as well as POC production were significantly higher in response to HL (Table 2, SI Table S3).

Regarding differential gene expression, numerous transcripts of conventional light harvesting antennae, mostly of the fucoxanthin/chlorophyll-binding protein (FCP) type, were rapidly and transiently downregulated in response to HL (Fig. 3a,b; SI Table S6), while antennae of the protective LI818 type were prominently upregulated (Fig. 3c,d; SI Table S6). Also, numerous transcripts related to photosynthetic electron transfer, especially the oxygen-evolving complex and the reaction center protein M of photosystem II (PSII) as well as subunits of the cytochrome b$_6$/f complex and ferredoxin-NADP$^+$-reductase were transiently downregulated in response to HL-exposure. Only few transcripts, e.g. the D1 protein and the stabilizing psbW subunit of PSII, as well as ferredoxin were upregulated (Fig. 3e,f; SI Table S6). A number of transcripts involved in chlorophyll synthesis (Fig. 3g,h; SI Table S6) were transiently downregulated due to HL-exposure, e.g. coproporphyrinogen III oxidase, Mg-protoporphyrin IX methyltransferase and uroporphyrinogen decarboxylase. Transcripts related to antioxidative protective mechanisms were prominently upregulated in response to HL-exposure (Fig. 3i,j; SI Table S6), especially of the glutathione system, like glutaredoxin, glutathione dehydrogenase and a glutathione S-transferase-like protein. Also, a number of transcripts related to the ascorbate system, e.g. ascorbate peroxidase and dehydroascorbate reductase, were significantly upregulated. One transcript related to Vitamin E synthesis, tocopherol o-methyltransferase, was

10

also upregulated. Few transcripts of the carbon metabolism were upregulated, amongst them e.g. two transcripts related to the synthesis of mycosporine-like amino acids (2-epi-5-epi-valiolone synthase, Fig. 3k,l). Transcripts related to lipid metabolism, many of which were desaturases, i.e. enzymes that introduce double bonds into acyl-chains, experienced an ambiguous regulation at 2 h, but were concertedly upregulated at 24 h and reverted to near-baseline expression levels after 120 h (Fig. 3m,n; SI Table S6).

HL-responses in N. frigida

N. frigida reacted faster and more strongly to HL exposure compared to *T. hyalina*, and did not achieve a successful acclimation to elevated light levels within the experiment. F_v/F_m was reduced from 0.53 ± 0.00 to 0.23 ± 0.03, i.e. by ~50% after only 15 min of HL-exposure and did not notably recover over the time course (Fig. 1g, SI Table S2). σ_{PSII} decreased gradually from 4.0 to 2.2 nm^2 $PSII^{-1}$ over 48 h of HL-exposure. Thereafter, no further changes in σ_{PSII} were detectable (Fig. 1h, SI Table S2). Also, NPQ increased immediately from 0.8 ± 0.0 to 3.3 ± 0.5 after only 15 min of HL-exposure (Fig. 2i), reached its highest level at 3 h (6.2 ± 1.2), and then gradually approached ~3.1 ± 0.1 over the rest of the time course (SI Table S2). α dropped from 0.7 ± 0.07 in LL to 0.2 ± 0.08 within 15 min of HL-exposure and did not recover until the end (Fig. 1j, SI Table S2). ETR did not change upon HL-exposure and remained at levels similar to the initial LL condition (32.2 ± 13.0 mol e^- (mol $RCII)^{-1}$ s^{-1}, Fig. 1k, SI Table S2). During the first 48 h of HL-exposure, E_k continuously increased from 82 ± 7 to 254 ± 30 µmol photons m^{-2} s^{-1} and stabilized at that level until the end of the time course (Fig. 1l, SI Table S2). HL-exposure significantly decreased cellular quotas of light harvesting pigments Chl*a*, fucoxanthin, Chl*c* 1+2 and Chl*c* 3 (Fig. 2c, SI Table S2). The cumulative quotas of the protective pigments DD+DT increased significantly after 24 h and beyond, resulting in almost five-fold higher DD+DT quotas in HL-acclimated cells compared to LL-acclimated cells (Fig. 2d, SI Table S2). Growth rates of *N. frigida* were significantly reduced as a consequence of HL-exposure, while POC and PON quotas as well as POC production remained at levels similar to LL-acclimated cells (Table 2, SI Table S3).

In response to HL-exposure, also *N. frigida* rapidly downregulated numerous transcripts of light harvesting proteins of the FCP type (Fig. 3o,p; SI Table S6). In contrast to *T. hyalina*, however, ~30 putative FCP-related light harvesting proteins were found strongly upregulated. Transcripts related to antennae of the protective LI818 type were prominently upregulated (Fig. 3q,r; SI Table S6), as seen in *T. hyalina*. Unlike in *T. hyalina*, upregulation of transcripts related to the

diatom xanthophyll cycle (homologs of zeaxanthin epoxidase, diadinoxanthin de-epoxidase) was detectable. As observed in *T. hyalina*, transcripts related to photosynthetic electron transfer, like subunits of the oxygen-evolving complex at PSII and reaction center protein psbM were downregulated, while the psbW and psbP proteins were upregulated (Fig. 3s,t; SI Table S6). Transcripts related to the synthesis of chlorophylls were, like in *T. hyalina*, transiently downregulated and gene expression re-established towards the end of the time course at a slightly higher level (Fig. 3u,v; SI Table S6). In response to HL-exposure, *N. frigida* slightly upregulated fewer and different transcripts related to oxidative stress detoxification than *T. hyalina*, in particular two transcripts related to Mn- and Cu/Zn-based superoxide dismutases as well as two transcripts related to vitamin E synthesis (tocopherol polyprenyltransferase-like protein) and membrane protection (probable phospholipid hydroperoxide glutathione peroxidase isoform X1; Fig. 3w,x; SI Table S6). In contrast to *T. hyalina*, only few transcripts related to the glutathione and ascorbate antioxidant systems were weakly regulated. Like in *T. hyalina*, transcripts related to lipid metabolism were ambiguously regulated: Several transcripts involved in lipogenesis, e.g. long chain acyl-CoA synthetase or the acyl carrier protein were downregulated, while other transcripts, especially those related to desaturases were upregulated, e.g. precursor of omega-3 desaturase, a generic acyl desaturase, dihydroceramide delta-4 desaturase and delta 9 desaturase (Fig. 3ä,ö; SI Table S6).

pCO_2 responses of both species

In *T. hyalina* cultures grown under LL, OA responses were generally subtle or completely absent. The photophysiological variables F_v/F_m, σ_{PSII}, NPQ, α, ETR and E_k did not show any statistically significant differences between 400 and 1000 µatm pCO_2 (Fig. 1a-f, SI Table S3). Chl*a*, fucoxanthin and Chl*c* 1+2 quotas were significantly higher in response to OA (Fig. 2a, SI Table S3). The cumulative quotas of DD+DT decreased under OA (from 36 ± 9 cell^{-1} to 24 ± 7 fg cell^{-1}; Fig. 2b), although lacking statistical significance. Also POC production, growth rates and POC and PON quotas remained statistically indifferent between low and high pCO_2 under LL conditions (Table 2, SI Table S3). Interestingly, when acclimated to HL, *T. hyalina* was responsive to high pCO_2. F_v/F_m values were significantly decreased under OA (Fig. 1a), while NPQ and DD+DT quotas (Fig. 1c and 2b) were significantly increased in cells acclimated to HL (SI Table S3). This translated into significantly lower growth rates under high pCO_2 (0.66 ± 0.14 d^{-1}) compared to low pCO_2 (0.92 ± 0.10 d^{-1}) for HL-acclimated cells (Table 2, SI Table S3). In contrast to *T. hyalina*, *N. frigida* responded to OA also when grown under LL: F_v/F_m and α (Fig. 1g,j) decreased significantly, in line with slightly decreased POC production under

high vs. low $p\text{CO}_2$ (3.2 ± 0.3 vs. 3.8 ± 0.2 pmol cell^{-1} d^{-1}; Table 2, SI Table S3). Overall, OA appeared to cause steeper responses in growth and biomass production in *N. frigida* at HL. For instance, growth rates as well as POC and PON production responded to HL, but under OA, the difference between both treatments were larger, and the responses therefore more intense (Table 2).

The gene expression changes in *T. hyalina* and *N. frigida* in response to $p\text{CO}_2$ alone were negligibly small, and no explicit regulation patterns could be identified besides that on average, transcripts experience a slightly lower expression: For *T. hyalina*, the average gene expression under elevated $p\text{CO}_2$ was 0.933, i.e. genes experienced ~7% downregulation under elevated $p\text{CO}_2$ (n=1849, regarding all transcripts with average RPKM ≥35; Fig. 4a). Regarding only those genes that could be successfully attributed to physiological processes, the average expression under elevated $p\text{CO}_2$ was 0.905 (n=998), reflecting a decrease in gene expression of ~10%. Only a negligible percentage of 2.5% of classified genes experienced a regulation ≥2-fold. In *N. frigida*, the average expression under elevated $p\text{CO}_2$ was 0.972, i.e. genes experienced ~3% downregulation under elevated $p\text{CO}_2$ (n=1362, regarding all transcripts with avg. RPKM ≥35; Fig. 4b). Regarding only those genes that could be successfully attributed to physiological processes, the average regulation under elevated $p\text{CO}_2$ was 0.944 (n=553), reflecting an average decrease in gene expression of only ~5%. The percentage of classified genes that experienced a regulation ≥2-fold was with 9.6% higher than in *T. hyalina*, but again, the resulting expression patterns did not point towards specific CO_2-sensitive processes.

Regarding the modulation of the HL-responses by $p\text{CO}_2$, data indicated that in *T. hyalina*, those transcripts that were upregulated in response to HL-stress generally experienced a *stronger* upregulation when cells were grown under high $p\text{CO}_2$ (Fig. 4c). When transcripts were downregulated in response to HL-stress, this downregulation was on average *less* intense, i.e. dampened by elevated $p\text{CO}_2$ (Fig. 4e). In *N. frigida*, this effect was even more apparent, where upregulations due to HL were on average up to ~50 fold stronger under high $p\text{CO}_2$, and downregulations were on average dampened to ~90% of their intensity (Fig. 4d,f).

Discussion

T. hyalina showed high resilience against high-light stress

T. hyalina´s response to HL could be divided into different phases, i.e. a short-term response (first 12 h), an intermediate recovery phase (24 - 72 h) and a re-acclimated state (>72 h), as

observed before for diatoms (Nymark *et al.*, 2009). Such acclimation dynamics were also well reflected in the time-course of gene expression, in which most genes initially showed a strong excursion of expression values (up- or downregulation) and a reversion or re-establishment of a new expression level over the course of acclimation (Fig. 3a-ö).

In the short-term response phase, *T. hyalina* throttled light harvesting to avoid photodamage: α decreased during the first 12 h (Fig. 1d), likely due to the uncoupling of antennae from reaction centers and an intensified package effect. This was also indicated by the peaking and gradual decrease in σ_{PSII} (Fig. 1b) and the upregulation of the psbW subunit that stabilizes the PSII and its antennae (García-Cerdán *et al.*, 2011). Also, an increased NPQ (Fig. 1c) was part of this typical diatom response to HL stress (Brunet *et al.*, 2011; Giovagnetti & Ruban, 2017) that was recognizable as well on the transcriptomic level: Cells rapidly decreased expression of conventional fucoxanthin-chlorophyll a/c-bearing proteins (FCPs; Fig. 3a,b) to reduce light harvesting. Concomitantly, cells induced FCP-homologs of the LI818 clade (Fig. 3c,d), thereby leveraging photoprotection by NPQ (Zhu & Green, 2010; Nymark *et al.*, 2013). Beyond this, *T. hyalina* also decreased expression of core components of PSII and the cytochrome b$_6$/f complex to maintain balanced photosynthetic electron transport despite higher excitation pressure. This ability to divert a higher fraction of excitons into harmless dissipation pathways and to accommodate the photosynthetic electron transfer chains was likely one reason for the constantly high ETR under HL-stress (Fig. 1e). The upregulation of the D1 protein (Fig. 3e,f) reflected the intense 'wear and tear' under HL-conditions (Galindo *et al.*, 2017): This protein is highly susceptible to oxidative damage, and its dysfunctional remnants act as inductors of its own gene expression (Tyystjärvi *et al.*, 1996).

T. hyalina´s intermediate response to HL involved the typical alteration of pigment composition (Brunet *et al.*, 2011). Significantly increased cumulative DD+DT quotas after 24 h of HL-exposure supported that *T. hyalina* synthesized photoprotective pigments as a countermeasure against the substantial HL-stress (Lavaud *et al.*, 2004). Although the expression of enzymes involved in chlorophyll synthesis was decreased at 2 h, recovered around 24 h and re-established at a higher level at 120 h (Fig. 3g,h), the measured chlorophyll quotas did not change significantly over the time course. Obviously, such changes do not directly manifest in changed phenotypes and exhibit a certain latency time (Nymark *et al.*, 2013). Remarkably, *T. hyalina* induced numerous genes related to the ascorbate and glutathione antioxidant systems under HL-stress (Fig. 3i,j). These dissipate oxidative stress by detoxification of hydrogen peroxide (H_2O_2), the main product of oxygen photoreduction and dismutation (Foyer & Noctor, 2011). The

pronounced regulation of these transcripts indicates that these systems are the prime defenses against oxidative stress in *T. hyalina*. Furthermore, the increased expression of a transcript related to the synthesis of vitamin E, a membrane-situated antioxidant that synergistically cooperates with the ascorbate system (Buettner, 1993), indicates that the avoidance of lipid damage from H_2O_2 is the second major strategy to cope with photophysiological stress. This is in line with the induction of multiple desaturases under HL, which increase the proportions of unsaturated fatty acids in organellar lipid bilayers. Desaturation of lipids causes a higher membrane fluidity, which increases the membrane-mobility of vitamin E (Los *et al.*, 2013) and eases the replacement of photosynthetic components. Two of the most prominently upregulated transcripts under HL-stress (>350 fold-change throughout the dataset) map to a 2-epi-5-epi-valiolone synthase-like enzyme, an enzyme involved in the synthesis of mycosporine-like amino acids. These aromatic molecules are found in literally all marine algae and protect cells from UV radiation and oxidative stress (Shick & Dunlap, 2002; Wada *et al.*, 2015). These data indicate that *T. hyalina* cells reacted to HL-exposure not only with decreased photon harvest and increased NPQ, but counteract oxidative stress with the concerted induction of effective antioxidant systems that are rooted at the 'heart of the cellular redox hub' (Foyer & Noctor, 2011). Furthermore, these findings corroborate that photosynthesis as a whole is a sensory-autoregulatory process (Pfannschmidt, 2003) and that redox-balance is its major regulator (Mittler, 2002; Stenbaek & Jensen, 2010). Despite the ability to cope well with photooxidative stress, several key variables reached minimal values during the course of the experiment at the 24 h time point (F_v/F_m, σ_{PSII}, α and ETR; Fig. 1a,b,d,e).

Beyond 48 h, *T. hyalina* entered the re-acclimation phase in which the operability of the photosynthetic machinery recovered, and F_v/F_m, α and ETR increased (Fig. 1a,d,e). At 72 h, *T. hyalina* was successfully acclimated to HL, exhibiting stabilized F_v/F_m, σ_{PSII}, NPQ, α and ETR, and with E_k having approached the HL intensity used in the experiments (Fig. 1a-f). HL-acclimated cells also increased in size, in line with higher POC quotas compared to LL (Table 2), which appears to be a common response of many phytoplankton species towards high irradiances (Thompson *et al.*, 1991). The increase in cell size also explains why cell-normalized light harvesting pigment quotas in HL were not lower than in LL, as would be expected after acclimation to higher irradiances. This became evident in the biomass-normalized pigment contents, which decreased by more than 50% in response to HL. The adjustments to the photosynthetic machinery, as discussed above, facilitated highly effective photosynthesis in

HL-acclimated *T. hyalina* cells, indicated by significantly higher growth rate and almost four times higher POC production (Table 2).

N. frigida exhibits higher sensitivity towards light stress

The short-term responses of *N. frigida* in the first 12 h were clearly different from *T. hyalina´*s. F_v/F_m and α decreased ~8 times faster in *N. frigida* than in *T. hyalina* (Fig. 1g,j), and much higher NPQ levels were measured (Fig. 1i). Like *T. hyalina*, *N. frigida* downregulated conventional FCPs (Fig. 3o,p) and upregulated photoprotective LI818 homologs (Fig. 3q,r). In line with the NPQ data, transcripts related to the xanthophyll cycle were prominently upregulated. However, ~30 conventional FCPs were indeed upregulated, which likely hampered the cells´ attempts to reduce photon harvest to the possible minimum. Also *N. frigida* downregulated components of PSII to decrease overall electron harvest, but the downregulation of ferredoxin-NADP$^+$-reductase (Fig. 3s,t), the terminal enzyme of photosynthetic light reactions, seemingly impaired electron drainage (Hartmann *et al.*, 2014). This explains the constantly high turnover times of the electron transfer chain (τ_{ES}, SI Fig. S1). Unlike *T. hyalina*, *N. frigida* did not prominently induce the ascorbate- and glutathione-related antioxidant systems, but rather upregulated comparably few transcripts of Mn- as well as Cu/Zn-based superoxide dismutases (Fig. 3w,x), which catalyze the conversion of superoxide radicals into H_2O_2. The different indicated metal-cofactors suggest that the regulated enzymes have different organellar location, and since oxidative stress regulates gene expression of antioxidant systems (Mittler, 2002), *N. frigida* apparently experienced oxidative stress in all major cellular compartments. The increased expression of a tocopherol polyprenyltransferase-like protein and a probable phospholipid hydroperoxide glutathione peroxidase (Fig. 3w,x) suggest that also *N. frigida* attempted to protect organellar membranes from oxidative stress and dangerous lipid-peroxidizing chain reactions (Pospíšil & Yamamoto, 2017). In line with this, *N. frigida* induced numerous desaturases (Fig. 3ä,ö). As in *T. hyalina*, these likely serve to increase fluidity in lipid bilayers, assisting repair of enzymatic machinery, enhancing the scavenging of oxidative stress by membrane-situated antioxidants, and creating unsaturated lipids that act as quenchers of oxidative stress themselves (Richard *et al.*, 2008; Los *et al.*, 2013).

Throughout the experiment, *N. frigida* did not achieve a proper acclimation to HL, and after 120 h, still experienced considerable stress and dysfunctional photosynthesis. By that time, the light harvesting pigment quotas had halved under HL compared to LL, despite *de novo* synthesis of photoprotective pigments at 120 h (Fig. 2c,d). *N. frigida* did not show any recovery

of the photosynthetic parameters F_v/F_m and α (Fig. 1g,j), and its ETR did not increase in response to HL, indicating that photoacclimative efforts were insufficient. As a consequence, growth rates were reduced and POC production could not profit from HL (Table 2). The continuous electron input and concomitant oxidative stress might have contributed to the stronger reduction in growth rate under HL. In conclusion, the combination of high sensitivity to photodamage, the inability to efficiently decrease light harvesting and lacking capacity to detoxify oxidative stress seem to have prevented a successful recovery and proper acclimation to HL in *N. frigida*. Despite these 'pathological' indications, the cells survived throughout the experiment. It therefore remains unclear whether they might successfully acclimate over longer time scales or with more gradual increases in irradiance. However, a clear negative impact of high irradiances on natural sea ice algal communities' biochemical composition has been documented earlier by Leu *et al.* (2010).

Although the striking differences between the photoacclimative capacities under HL-exposure of the two species was surprising, they could be attributed to the occupation of strongly contrasting ecological niches. Vertical mixing of phytoplankton cells in open water can induce fluctuations in light intensity at comparably short timescales, coupled with high amplitudes, while sympagic algae usually experience more gradually changing irradiances with much lower amplitude when snow and ice melt (Hill *et al.*, 2018). As a consequence, *T. hyalina* seems to have evolved more pronounced mechanisms to deal with rapid exposure to HL compared to *N. frigida*.

Light responses were modulated by ocean acidification

In *T. hyalina*, OA responses under LL were generally subtle, e.g. in POC production and quotas of light harvesting pigments (Table 2; Fig. 2a), or even completely absent, e.g. in physiological responses (F_v/F_m, σ_{PSII}, α, ETR and E_k, Fig. 1a-f). This is in line with the notion that this species exhibits a high physiological plasticity and a broad niche over a range of pCO$_2$ (Wolf *et al.*, 2018). Under HL, however, significantly lower growth rates were observed in response to high pCO$_2$, indicating that combined HL and OA impose negative synergistic effects, as has been observed in previous studies (Gao *et al.*, 2012; Hoppe *et al.*, 2015). Also, significantly higher NPQ and increased quotas of xanthophyll cycle pigments (Fig. 1c,2b) suggest a higher level of stress under combined OA and HL, despite *T. hyalina*´s ability to compensate. The oxidative stress derived from HL-exposure and the concomitant increase of [CO$_2$] and/or H$^+$ levels seems to impair overall cellular homeostasis, making it more difficult for cells to adjust redox

harmonics. Thus, it may be interpreted that the generally wide CO_2 niche of *T. hyalina* gets slightly narrower under HL.

N. frigida was not only more responsive to HL, but also to OA: Cells grown under high pCO_2 showed reduced F_v/F_m and α, which translated into lower POC production under OA irrespective of light level (Fig. 1g,j; Table 2). Regarding growth rates, OA caused beneficial effects under LL, but detrimental effects under HL (Table 2). Despite the fact that growth rate and POC production seem to be affected differently, i.e. have differently shaped reaction norms, this indicates a narrower CO_2 niche of *N. frigida* compared to *T. hyalina*, which is constricted even further by HL. It seems plausible that in *N. frigida* cells, low pH caused distorted ion homeostasis and signalling (Rokitta *et al.*, 2012), which might have additionally hampered re-acclimation.

The effects of OA on the gene expression patterns of both species were ambiguous with respect to biochemical pathways and cellular functions, which is in line with absence of concrete pCO_2 effects in pelagic assemblages from diverse Arctic habitats (Hoppe *et al.*, 2018). More importantly, the changes of gene expression induced by elevated pCO_2 were so small that an evaluation was pointless, also because the used experimental setup, replication and sequencing depth would require changes >2-fold to make any reliable statements (Conesa *et al.*, 2016), which was the case for only 2.5% or 9.6% of the data of *T. hyalina* or *N. frigida*, respectively (Fig. 4a,b). Thus, it can only be said that high pCO_2 seemingly lowered the 'on average' expression of transcripts across the dataset, an effect that appears to be stronger in *T. hyalina* (on average 10% lower expression under high pCO_2) than in *N. frigida* (on average 5% lower expression under high pCO_2).

The pCO_2-modulation of transcriptomic HL-responses was similarly ambiguous. In both species, elevated pCO_2 modulated the HL-responses to be on average stronger for upregulated genes, and weaker for downregulated genes (Fig. 4c-f). This especially holds true for the majority of the upregulated photoprotective antennae of the LI818-type, the transcripts related to mycosporine-like amino acids synthesis, as well as for the downregulated FCP-like light harvesting antennae, which explains why the photophysiological responses (e.g. NPQ) of both species under HL and OA are more pronounced. As pCO_2 alone does not cause specific expression patterns, it can be deduced that OA imposes secondary effects on the cells, likely by altering the substrate availability and chemical conditions within or between organelles, or by affecting physiological signals like membrane potentials or redox equilibria (Rokitta *et al.*,

2012). Thus, despite the species´ different capacities to cope with HL-stress, OA seems to impose an additional stress that requires more intense regulatory efforts. While this phenomenon did not change the overall picture gained from the two physiologically and evolutionarily distinct microalgae used here, future environmental change, especially the combination of HL-stress and OA is likely to negatively affect the ecological performance of microalgae and restrict habitat occupation and niche partitioning in the Arctic.

Conclusion

T. hyalina, with its robust light harvesting apparatus and efficient antioxidant systems handled photophysiological stress well and acclimated rapidly to higher irradiances, leading to increased growth rates and organic carbon quotas under HL-conditions. In *N. frigida*, in contrast, photochemical damage and oxidative stress appeared to overweigh cellular defenses, causing dysfunctional photophysiology and reduced fitness with decreased photosynthetic yields, ETR and growth rates. OA increased these sensitivities to HL-stress in both species, highlighting the importance of interacting environmental variables. Despite the overarching nature of these interactions, we found substantial differences in sensitivity between pelagic and sympagic diatoms, which could significantly alter their relative contribution to biomass and annual primary production in a future Arctic. *T. hyalina* will likely continue to be a major primary producer in the pelagic realm, which is furthermore becoming more prevalent (Stroeve & Notz, 2018). Due to the increasing importance of ephemeral, i.e. melting and re-forming sea ice (Onarheim *et al.*, 2018), environmental dynamics encountered by sympagic algae may become more similar to what pelagic organisms experience. Our results indicate a decrease in fitness of important sea-ice algae in response to climate change, potentially altering colonization and productivity in Arctic sea ice with negative effects on downstream food webs. Their differential sensitivity towards climate change needs to be incorporated into scenarios of future Arctic algae blooms, including implications for the ecosystem.

Acknowledgements

Author contribution

ACK, EL, BR, SDR and CJMH initially planned the experimental approach; ACK and CJMH conducted lab cultivations and collected samples; ACK processed and evaluated the FRRf, pigment and elemental data. SDR processed RNA samples, conducted the sequencing, processed and evaluated the data; LH assembled the de-novo transcriptome and assisted in bioinformatical post-processing; ACK and SDR drafted the manuscript; All authors contributed to writing the final manuscript.

References

Aletsee L, Jahnke J. 1992. Growth and productivity of the psychrophilic marine diatoms *Thalassiosira antarctica* Comber and *Nitzschia frigida* Grunow in batch cultures at temperatures below the freezing point of sea water. *Polar biology* **11**(8): 643-647.

Alou-Font E, Roy S, Agustí S, Gosselin M. 2016. Cell viability, pigments and photosynthetic performance of Arctic phytoplankton in contrasting ice-covered and open-water conditions during the spring-summer transition. *Marine Ecology Progress Series* **543**: 89-106.

Altschul SF, Gish W, Miller W, Myers EW, Lipman DJ. 1990. Basic local alignment search tool. *Journal of Molecular Biology* **215**(3): 403-410.

AMAP. 2013. *Arctic Monitoring and Assessment Programme; Assessment 2013: Arctic Ocean Acidification*. Oslo, Norway.

Andrew S. 2010. FastQC: A quality control tool for high throughput sequence data. http://www.bioinformatics.babraham.ac.uk/projects/fastqc.

Benjamini Y, Hochberg Y. 1995. Controlling the false discovery rate - a practical and powerful approach to multiple testing. *Journal of the Royal Statistical Society Series B-Methodological* **57**(1): 289-300.

Brunet C, Johnsen G, Lavaud J, Roy S. 2011. Pigments and photoacclimation processes. In: Roy S, Llewellyn CA, Egelang ES, Johnsen G, eds. *Phytoplankton Pigments: Characterization, Chemotaxonomy and Applications in Oceanography*. Cambridge, UK: Cambridge University press, 445-454.

Buettner GR. 1993. The Pecking Order of Free Radicals and Antioxidants: Lipid Peroxidation, α-Tocopherol, and Ascorbate. *Archives of Biochemistry and Biophysics* **300**(2): 535-543.

Bushnell B. 2015. BBMap short read aligner, and other bioinformatic tools. http://sourceforge.net/projects/bbmap

Conesa A, Madrigal P, Tarazona S, Gomez-Cabrero D, Cervera A, McPherson A, Szcześniak MW, Gaffney DJ, Elo LL, Zhang X, et al. 2016. A survey of best practices for RNA-seq data analysis. *Genome Biology* **17**: 13.

Eilers PHC, Peeters JCH. 1988. A model for the relationship between light intensity and the rate of photosynthesis in phytoplankton. *Ecological Modelling* **42**(3): 199-215.

Foyer CH, Noctor G. 2011. Ascorbate and glutathione: The heart of the redox hub. *Plant Physiology* **155**(1): 2-18.

Galindo V, Gosselin M, Lavaud J, Mundy CJ, Else B, Ehn J, Babin M, Rysgaard S. 2017. Pigment composition and photoprotection of Arctic sea ice algae during spring. *Marine Ecology Progress Series* **585**: 49-69.

Gao K, Campbell DA. 2014. Photophysiological responses of marine diatoms to elevated CO_2 and decreased pH: a review. *Functional Plant Biology* **41**(5): 449-459.

Gao K, Xu J, Gao G, Li Y, Hutchins DA, Huang B, Wang L, Zheng Y, Jin P, Cai X, et al. 2012. Rising CO_2 and increased light exposure synergistically reduce marine primary productivity. *Nature Climate Change* **2**(7): 519-523.

García-Cerdán JG, Kovács L, Tóth T, Kereïche S, Aseeva E, Boekema EJ, Mamedov F, Funk C, Schröder WP. 2011. The PsbW protein stabilizes the supramolecular organization of photosystemII in higher plants. *The Plant Journal* **65**(3): 368-381.

Giordano M, Beardall J, Raven JA. 2005. CO_2 concentrating mechanisms in algae: mechanisms, environmental modulation, and evolution. *Annual Review of Plant Biology* **56**: 99-131.

Giovagnetti V, Ruban AV. 2017. Detachment of the fucoxanthin chlorophyll a/c binding protein (FCP) antenna is not involved in the acclimative regulation of photoprotection in the pennate diatom *Phaeodactylum tricornutum*. *Biochimica et Biophysica Acta-Bioenergetics* **1858**: 218-230.

Grabherr MG, Haas BJ, Yassour M, Levin JZ, Thompson DA, Amit I, Adiconis X, Fan L, Raychowdhury R, Zeng Q, et al. 2011. Full-length transcriptome assembly from RNA-Seq data without a reference genome. *Nature Biotechnology* **29**: 644.

Guillard RR, Ryther JH. 1962. Studies of marine planktonic diatoms: I. *Cyclotella nana* Hustedt, and *Detonula confervacea* (Cleve) Gran. *Canadian journal of microbiology* **8**: 229-239.

Hancke K, Lund-Hansen LC, Lamare ML, Højlund Pedersen S, King MD, Andersen P, Sorrell BK. 2018. Extreme low light requirement for algae growth underneath sea ice: A case study from station Nord, NE Greenland. *Journal of Geophysical Research: Oceans* **123**(2): 985-1000.

Hartmann P, Béchet Q, Bernard O. 2014. The effect of photosynthesis time scales on microalgae productivity. *Bioprocess and Biosystems Engineering* **37**(1): 17-25.

Hegseth EN, Sundfjord A. 2008. Intrusion and blooming of Atlantic phytoplankton species in the high Arctic. *Journal of Marine Systems* **74**(1–2): 108-119.

Hill VJ, Light B, Steele M, Zimmerman RC. 2018. Light Availability and Phytoplankton Growth Beneath Arctic Sea Ice: Integrating Observations and Modeling. *Journal of Geophysical Research: Oceans* **123**(5): 3651-3667.

Hopkinson BM, Dupont CL, Allen AE, Morel FMM. 2011. Efficiency of the CO_2-concentrating mechanism of diatoms. *Proceedings of the National Academy of Sciences* **108**(10): 3830-3837.

Hoppe CJM, Holtz L-M, Trimborn S, Rost B. 2015. Ocean acidification decreases the light-use efficiency in an Antarctic diatom under dynamic but not constant light. *New Phytologist* **207**(1): 159-171.

Hoppe CJM, Wolf KKE, Schuback N, Tortell PD, Rost B. 2018. Compensation of ocean acidification effects in Arctic phytoplankton assemblages. *Nature Climate Change* **8**(6): 529-533.

IPCC 2014. Summary for Policymakers. In: Field CB, Barros VR, Dokken DJ, Mach KJ, Mastrandrea MD, Bilir TE, Chatterjee M, Ebi KL, Estrada YO, Genova RC, Girma B, Kissel ES, Levy AN, MacCracken S, Mastrandrea PR, White LL eds. *Climate Change 2014: Impacts, Adaptation, and Vulnerability. Part A: Global and Sectoral Aspects. Contribution of Working Group II to the Fifth Assessment Report of the Intergovernmental Panel on Climate Change*. Cambridge, United Kingdom, and New York, NY, USA: Cambridge University Press, 1-32.

Kopylova E, Noé L, Touzet H. 2012. SortMeRNA: fast and accurate filtering of ribosomal RNAs in metatranscriptomic data. *Bioinformatics* **28**(24): 3211-3217.

Kroeker KJ, Kordas RL, Crim R, Hendriks IE, Ramajo L, Singh GS, Duarte CM, Gattuso JP. 2013. Impacts of ocean acidification on marine organisms: quantifying sensitivities and interaction with warming. *Global Change Biology* **19**: 1884-1896.

Lavaud J, Goss R. 2014. The peculiar features of non-photochemical fluorescence quenching in diatoms and brown algae. In: Demmig-Adams B, Garab G, Adams III W, Govindjee, eds. *Non-photochemical quenching and energy dissipation in plants, algae and cyanobacteria*. Dordrecht, Netherlands: Springer, 421-443.

Lavaud J, Rousseau B, Etienne AL. 2004. General features of photoprotection by energy dissipation in planktonic diatoms (Bacillariophyceae). *Journal of phycology* **40**(1): 130-137.

Leu E, Wiktor J, Søreide J, Berge J, Falk-Petersen S. 2010. Increased irradiance reduces food quality of sea ice algae. *Marine Ecology Progress Series* **411**: 49-60.

Leu E, Mundy C, Assmy P, Campbell K, Gabrielsen T, Gosselin M, Juul-Pedersen T, Gradinger R. 2015. Arctic spring awakening–Steering principles behind the phenology of vernal ice algal blooms. *Progress in Oceanography* **139**: 151-170.

Li G, Campbell DA. 2013. Rising CO_2 interacts with growth light and growth rate to alter photosystem II photoinactivation of the coastal diatom *Thalassiosira pseudonana*. *PloS one* **8**: e55562.

Light B, Perovich DK, Webster MA, Polashenski C, Dadic R. 2015. Optical properties of melting first-year Arctic sea ice. *Journal of Geophysical Research: Oceans* **120**(11): 7657-7675.

Los DA, Mironov KS, Allakhverdiev SI. 2013. Regulatory role of membrane fluidity in gene expression and physiological functions. *Photosynthesis Research* **116**(2): 489-509.

MacIntyre HL, Kana TM, Geider RJ. 2000. The effect of water motion on short-term rates of photosynthesis by marine phytoplankton. *Trends in Plant Science* **5**(1): 12-17.

McCarthy A, Rogers SP, Duffy SJ, Campbell DA. 2012. Elevated carbon dioxide differentially alters the photophysiology of *Thalassiosira pseudonana* (Bacillariophyceae) and *Emiliania huxleyi* (Haptophyta). *Journal of Phycology* **48**(3): 635-646.

McMinn A. 2017. Reviews and syntheses: Ice acidification, the effects of ocean acidification on sea ice microbial communities. *Biogeosciences* **14**(17): 3927.

McMinn A, Müller MN, Martin A, Ryan KG. 2014. The Response of Antarctic Sea Ice Algae to Changes in pH and CO_2. *PLOS ONE* **9**(1): e86984.

Mittler R. 2002. Oxidative stress, antioxidants and stress tolerance. *Trends in Plant Science* **7**(9): 405-410.

Mortazavi A, Williams BA, McCue K, Schaeffer L, Wold B. 2008. Mapping and quantifying mammalian transcriptomes by RNA-Seq. *Nature Methods* **5**: 621.

Nicolaus M, Katlein C, Maslanik J, Hendricks S. 2012. Changes in Arctic sea ice result in increasing light transmittance and absorption. *Geophysical Research Letters* **39**: L24501, doi: 10.1029/2012GL053738

Nymark M, Valle KC, Brembu T, Hancke K, Winge P, Andresen K, Johnsen G, Bones AM. 2009. An integrated analysis of molecular acclimation to high light in the marine diatom *Phaeodactylum tricornutum*. *PloS one* **4**: e7743.

Nymark M, Valle KC, Hancke K, Winge P, Andresen K, Johnsen G, Bones AM, Brembu T. 2013. Molecular and photosynthetic responses to prolonged darkness and subsequent

acclimation to re-Illumination in the diatom *Phaeodactylum tricornutum*. *PloS one* **8**(3): e58722.

Onarheim IH, Eldevik T, Smedsrud LH, Stroeve JC. 2018. Seasonal and regional manifestation of Arctic sea ice loss. *Journal of Climate* **31**: 4917-4932.

Oxborough K, Moore CM, Suggett DJ, Lawson T, Chan HG, Geider RJ. 2012. Direct estimation of functional PSII reaction center concentration and PSII electron flux on a volume basis: a new approach to the analysis of Fast Repetition Rate fluorometry (FRRf) data. *Limnology and Oceanography Methods* **10**: 142-154.

Pfannschmidt T. 2003. Chloroplast redox signals: how photosynthesis controls its own genes. *Trends in Plant Science* **8**(1): 33-41.

Pierrot DE, Lewis E, Wallace DWR. 2006. *MS excel program developed for CO_2 system calculations. ORNL/OCDIAC-105a carbon dioxide information analysis centre.* ORNL, TN, USA: US Department of Energy.

Pospíšil P, Yamamoto Y. 2017. Damage to photosystem II by lipid peroxidation products. *Biochimica et Biophysica Acta (BBA) - General Subjects* **1861**(2): 457-466.

Poulin M, Daugbjerg N, Gradinger R, Ilyash L, Ratkova T, von Quillfeldt C. 2011. The pan-Arctic biodiversity of marine pelagic and sea-ice unicellular eukaryotes: a first-attempt assessment. *Marine Biodiversity* **41**(1): 13-28.

Richard D, Kefi K, Barbe U, Bausero P, Visioli F. 2008. Polyunsaturated fatty acids as antioxidants. *Pharmacological Research* **57**(6): 451-455.

Robinson MD, McCarthy DJ, Smyth GK. 2010. edgeR: a Bioconductor package for differential expression analysis of digital gene expression data. *Bioinformatics* **26**(1): 139-140.

Robinson MD, Oshlack A. 2010. A scaling normalization method for differential expression analysis of RNA-seq data. *Genome Biology* **11**(3): R25.

Rodriguez F, Chauton M, Johnsen G, Andresen K, Olsen L, Zapata M. 2006. Photoacclimation in phytoplankton: implications for biomass estimates, pigment functionality and chemotaxonomy. *Marine Biology* **148**(5): 963-971.

Rokitta SD, John U, Rost B. 2012. Ocean Acidification affects redox-balance and ion-homeostasis in the life-cycle stages of *Emiliania huxleyi*. *PloS one* **7**(12): e52212.

Rost B, Riebesell U, Sültemeyer D. 2006. Carbon acquisition of marine phytoplankton: effect of photoperiod length. *Limnology and Oceanography* **51**: 12-20.

Rost B, Zondervan I, Wolf-Gladrow D. 2008. Sensitivity of phytoplankton to future changes in ocean carbonate chemistry: Current knowledge, contradictions and research directions. *Marine Ecology Progress Series* **373**: 227-237.

Screen JA, Simmonds I. 2010. The central role of diminishing sea ice in recent Arctic temperature amplification. *Nature* **464**(7293): 1334-1337.

Shick JM, Dunlap WC. 2002. Mycosporine-Like Amino Acids and Related Gadusols: Biosynthesis, Accumulation, and UV-Protective Functions in Aquatic Organisms. *Annual Review of Physiology* **64**(1): 223-262.

Stenbaek A, Jensen PE. 2010. Redox regulation of chlorophyll biosynthesis. *Phytochemistry* **71**(8): 853-859.

Stoll MHC, Bakker K, Nobbe GH, Haese RR. 2001. Continuous-Flow Analysis of Dissolved Inorganic Carbon Content in Seawater. *Analytical Chemistry* **73**(17): 4111-4116.

Stroeve JC, Notz D. 2018. Changing state of Arctic sea ice across all seasons. *Environmental Research Letters* **13**: 103001.

Syvertsen EE. 1991. Ice algae in the Barents Sea: types of assemblages, origin, fate and role in the ice-edge phytoplankton bloom. *Polar Research* **10**(1): 277-288.

Thompson PA, Harrison PJ, Parslow JS. 1991. Influence of irradiance on cell volume and carbon quota for ten species of marine phytoplankton. *Journal of phycology* **27**(3): 351-360.

Tremblay J-É, Anderson LG, Matrai P, Coupel P, Bélanger S, Michel C, Reigstad M. 2015. Global and regional drivers of nutrient supply, primary production and CO_2 drawdown in the changing Arctic Ocean. *Progress in Oceanography* **139**: 171-196.

Trimborn S, Wolf-Gladrow D, Richter K-U, Rost B. 2009. The effect of $p$$CO_2$ on carbon acquisition and intracellular assimilation in four marine diatom species. *Journal of Experimental Marine Biology and Ecology* **376**(1): 26-36.

Tyystjärvi T, Mulo P, Mäenpää P, Aro E-M. 1996. D1 polypeptide degradation may regulate psbA gene expression at transcriptional and translational levels in *Synechocystis* sp. PCC 6803. *Photosynthesis Research* **47**(2): 111-120.

Wada N, Sakamoto T, Matsugo S. 2015. Mycosporine-Like Amino Acids and Their Derivatives as Natural Antioxidants. *Antioxidants* **4**(3): 603.

Weeks WF, Ackley SF. 1986. The growth, structure, and properties of sea ice. In: Untersteiner N, ed. *The Geophysics of Sea Ice*. Boston, MA: Springer US, 9-164.

Wolf KK, Hoppe CJ, Rost B. 2018. Resilience by diversity: large intraspecific differences in climate change responses of an Arctic diatom. *Limnology and Oceanography* **63**(1): 397-411.

Yamamoto-Kawai M, McLaughlin FA, Carmack EC, Nishino S, Shimada K. 2009. Aragonite Undersaturation in the Arctic Ocean: Effects of Ocean Acidification and Sea Ice Melt. *Science* **326**(5956): 1098-1100.

Zhu S-H, Green BR. 2010. Photoprotection in the diatom *Thalassiosira pseudonana*: Role of LI818-like proteins in response to high light stress. *Biochimica et Biophysica Acta (BBA) - Bioenergetics* **1797**(8): 1449-1457.

Table 1. Seawater carbonate chemistry at the end of the treatments (n = 4; mean ± 1 SD). The carbonate system was calculated from DIC, pH, salinity (32.7), temperature (3°C), phosphate (6.3 µmol kg^{-1}) and silicate (100 kg^{-1}) using the CO$_2$Sys program (Pierrot *et al.*, 2006). Four control bottles that contained sterile medium were aerated with pCO$_2$ of 400 and 1000 µatm and sampled at the same time as *Thalassiosira hyalina* and *Nitzschia frigida*. Asterisks (*) indicate n = 3; mean ± 1 SD.

			Measured analytically			Calculated with CO$_2$SYS	
Species	Light	Target pCO$_2$ [µatm]	pH total scale	TA [µmol kg^{-1}]	DIC [µmol kg^{-1}]	Dissolved CO$_2$ [µmol kg^{-1}]	pCO$_2$ [µatm]
T. hyalina	LL	400	8.09 ± 0.01	2540 ± 11	2327 ± 12	21.7 ± 0.2	384 ± 3
T. hyalina	HL	400	8.15 ± 0.05	2529 ± 81	2236 ± 71	17.9 ± 2.5	316 ± 44
Control		400	8.09	2493	2268	20.9	362
T. hyalina	LL	1000	7.71 ± 0.01	2518 ± 33	2388 ± 25	53.9 ± 1.0	952 ± 18
T. hyalina	HL	1000	7.77 ± 0.05	2558 ± 14	2330 ± 32	45.7 ± 5.5	807 ± 98
Control		1000	7.74	2510	2360	49.71	857
N. frigida	LL	400	8.09 ± 0.01	2794 ± 30	2449 ± 18	22.9 ± 0.7	405 ± 12
N. frigida	HL	400	8.10 ± 0.01*	2759 ± 50*	2456 ± 11*	22.3 ± 0.5*	393 ± 8*
Control		400	8.07	2593	2477	23.8	413
N. frigida	LL	1000	7.68 ± 0.03*	2846 ± 9*	2513 ± 9*	61.6 ± 3.4*	1088 ± 60*
N. frigida	HL	1000	7.73 ± 0.01	2771 ± 66	2483 ± 13	53.9 ± 1.1	951 ± 20
Control		1000	7.71	2723	2507	56.1	967

Table 2. Growth rates, cellular quotas of particulate organic carbon and nitrogen (POC/PON) and POC production (n = 4; mean ± 1 SD), in addition to cell size (n = 30; mean ± 1 SD) of *Thalassiosira hyalina* and *Nitzschia frigida* at low-light (LL) and high-light (HL) under two pCO_2 levels (400 µatm and 1000 µatm). Asterisks (*) indicate n = 3; mean ± 1 SD.

Species	Light	pCO_2 [µatm]	Growth rate µ [d^{-1}]	POC [pmol cell^{-1}]	PON [pmol cell^{-1}]	POC production [pmol cell^{-1} d^{-1}]	Chl$a$:POC [g g^{-1} *1000]	Cell size [µm]
T. hyalina	LL	400	0.72 ± 0.10	24.5 ± 4.9	4.4 ± 1.1	15.4 ± 0.9	2.13 ± 0.18*	21.6 ± 2.1
T. hyalina	HL	400	0.92 ± 0.10*	61.8 ± 6.5	12.4 ± 1.4	59.2 ± 10.6	1.11 ± 0.15	27.4 ± 2.6
T. hyalina	LL	1000	0.62 ± 0.07	33.6 ± 7.9	6.4 ± 1.3	23.3 ± 5.5	2.43 ± 0.52*	20.6 ± 2.5
T. hyalina	HL	1000	0.66 ± 0.14	68.3 ± 19.0	13.5 ± 3.9	44.6 ± 15.7	1.40 ± 0.33	26.4 ± 3.0
N. frigida	LL	400	0.26 ± 0.02	14.7 ± 1.0	1.8 ± 0.2	3.8 ± 0.2	1.79 ± 0.26	7.5 ± 1.0
N. frigida	HL	400	0.22 ± 0.01*	17.0 ± 0.1*	2.2 ± 0.1*	3.9 ± 0.1*	0.75 ± 0.03*	7.0 ± 1.2
N. frigida	LL	1000	0.37 ± 0.05	9.1 ± 1.5	1.3 ± 0.2	3.2 ± 0.3	N/A	5.9 ± 0.6
N. frigida	HL	1000	0.15 ± 0.00*	31.8 ± 24.4*	4.2 ± 3.4*	2.7 ± 0.8*	0.50 ± 0.08*	6.7 ± 0.9

Figure legends

Fig. 1. Temporal changes of dark-acclimated maximum quantum yield of fluorescence (F_v/F_m; a,g), absorption cross section of photosystem II (σ_{PSII}; b,h), non-photochemical quenching in dark acclimated cells (NPQ; c,i), light utilization coefficient (α; d,j), relative electron transport rate at applied high-light irradiance (ETR; e,k) and light saturation index (E_k; f,l) in *Thalassiosira hyalina* (a-f, blue) and *Nitzschia frigida* (g-l, green). Cells were grown at 400 µatm (dark color) and 1000 µatm $p\mathrm{CO}_2$ (light color) in low-light (time point 0) and after 1, 2, 3, 4, 5, 6, 12, 24, 48, 72, 96 and 120 h of high-light exposure.

Fig. 2. Light harvesting pigment quotas (Chl*a*, fucoxanthin, Chl*c* 1+2 and Chl*c* 3; a,c) as well as light protective pigment quotas (diadinoxanthin and diatoxanthin, DD+DT; b,d) in *Thalassiosira hyalina* (a,b, blue) and *Nitzschia frigida* (c,d, green) at $p\mathrm{CO}_2$ levels of 400 µatm (without pattern) and 1000 µatm (with pattern). Pigment content was analyzed in low-light (time point 0) and high-light (time point 120) acclimated cells, as well as after 2 h and 24 h of HL exposure ($n \geq 3 \pm 1$ SD).

Fig. 3. Time course of gene expression changes in *Thalassiosira hyalina* (a-n, blue) and *Nitzschia frigida* (o-ö, green) under low (400 µatm; left panels) and high (1000 µatm; right panels) $p\mathrm{CO}_2$. Color intensity codes the overall expression levels, based on average numbers of reads per kilobase per million mapped nucleotides (RPKM) across the time course. Labels on the right represent functional classification.

Fig. 4. Histograms representing the expression values of identified and classified transcripts in *Thalassiosira hyalina* (a, blue, n=1857) and *Nitzschia frigida* (b, green, n=1358) in response to elevated $p\mathrm{CO}_2$, where the dashed line represents 1, i.e. no expression change. Bottom four graphs show the time course of $p\mathrm{CO}_2$-mediated relative intensity modulation of the light stress response for upregulated (c,d) and downregulated (e,f) genes in *Thalassiosira hyalina* (left; c,e) and *Nitzschia frigida* (right; d,f). Color intensity codes the overall expression levels, based in averaged numbers of reads per kilobase per million mapped nucleotides (RPKM) across the time courses in both $p\mathrm{CO}_2$ levels.

Supporting information

Fig S1: Temporal changes of the turnover time of the electron transfer chain (τ_{ES}) in *Thalassiosira hyalina* (closed circles, blue) and *Nitzschia frigida* (open circles, green) in low-light (time 0) and after 1, 2, 3, 4, 5, 6, 12, 24, 48, 72, 96 and 120 h of HL exposure.

Table S1: Details on FRRf assay settings applied in this study.

Table S2: Statistical results from repeated measures (RM) ANOVA analysis on the temporal development of photophysiological parameters after low- to high-light switch.

Table S3: Statistical results from Two-way ANOVA analysis comparing low and high-light acclimated treatments.

Table S4: Experiment metadata, including sample list as well as descriptive statistics regarding sequencing and post-processing.

Table S5: List of de-novo assembled transcripts obtained for the two species.

Table S6: Excel sheet containing expression data, results statistical significance tests, BLAST annotations as well as functional classification.
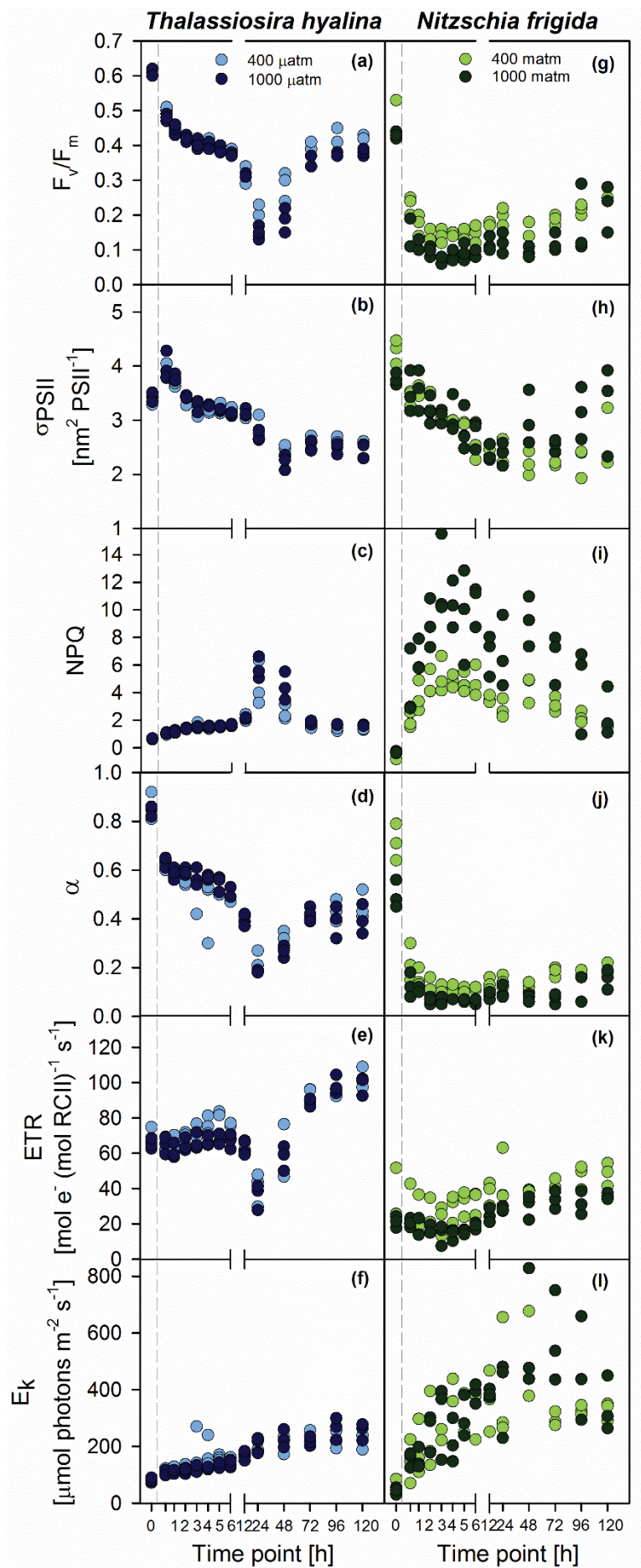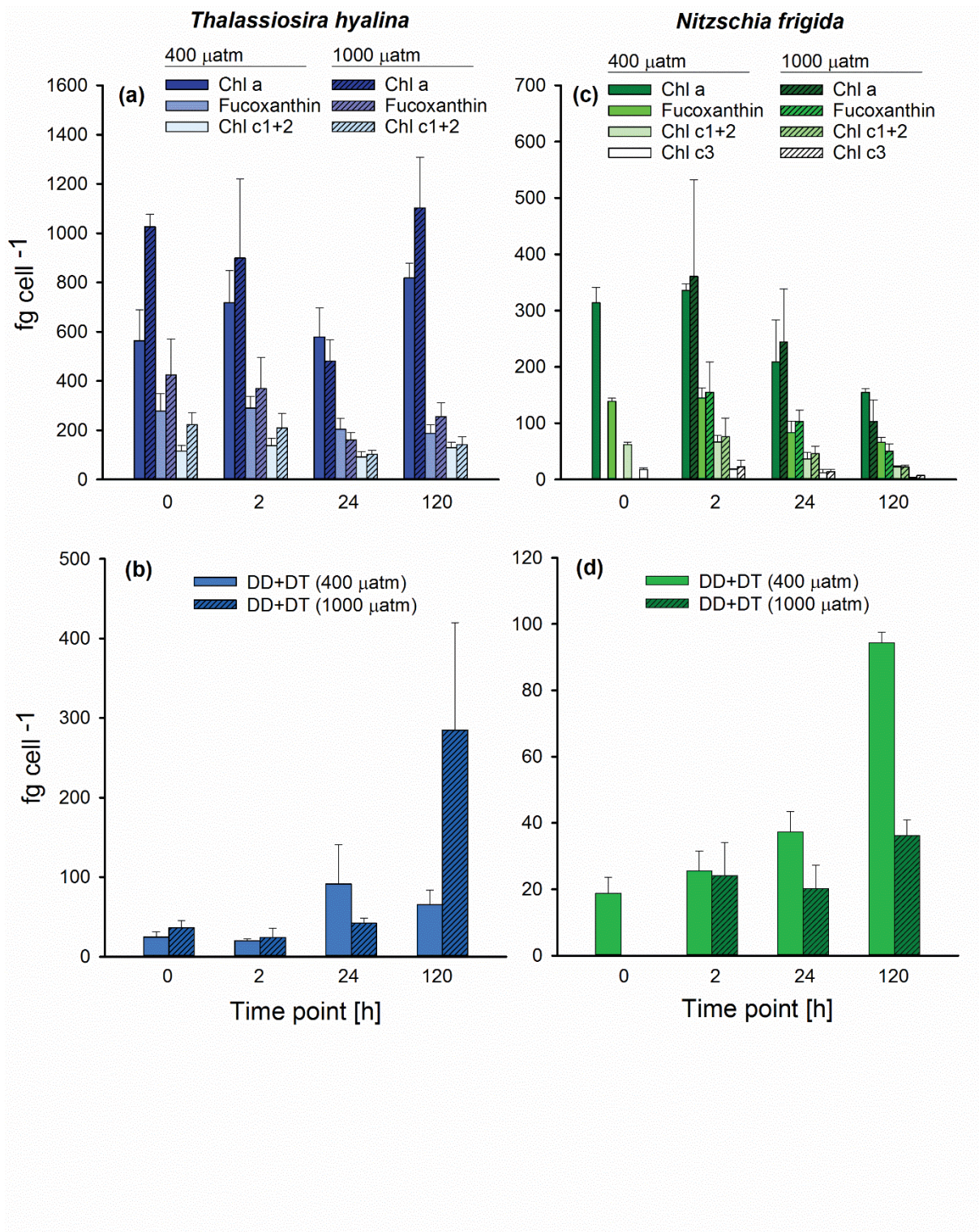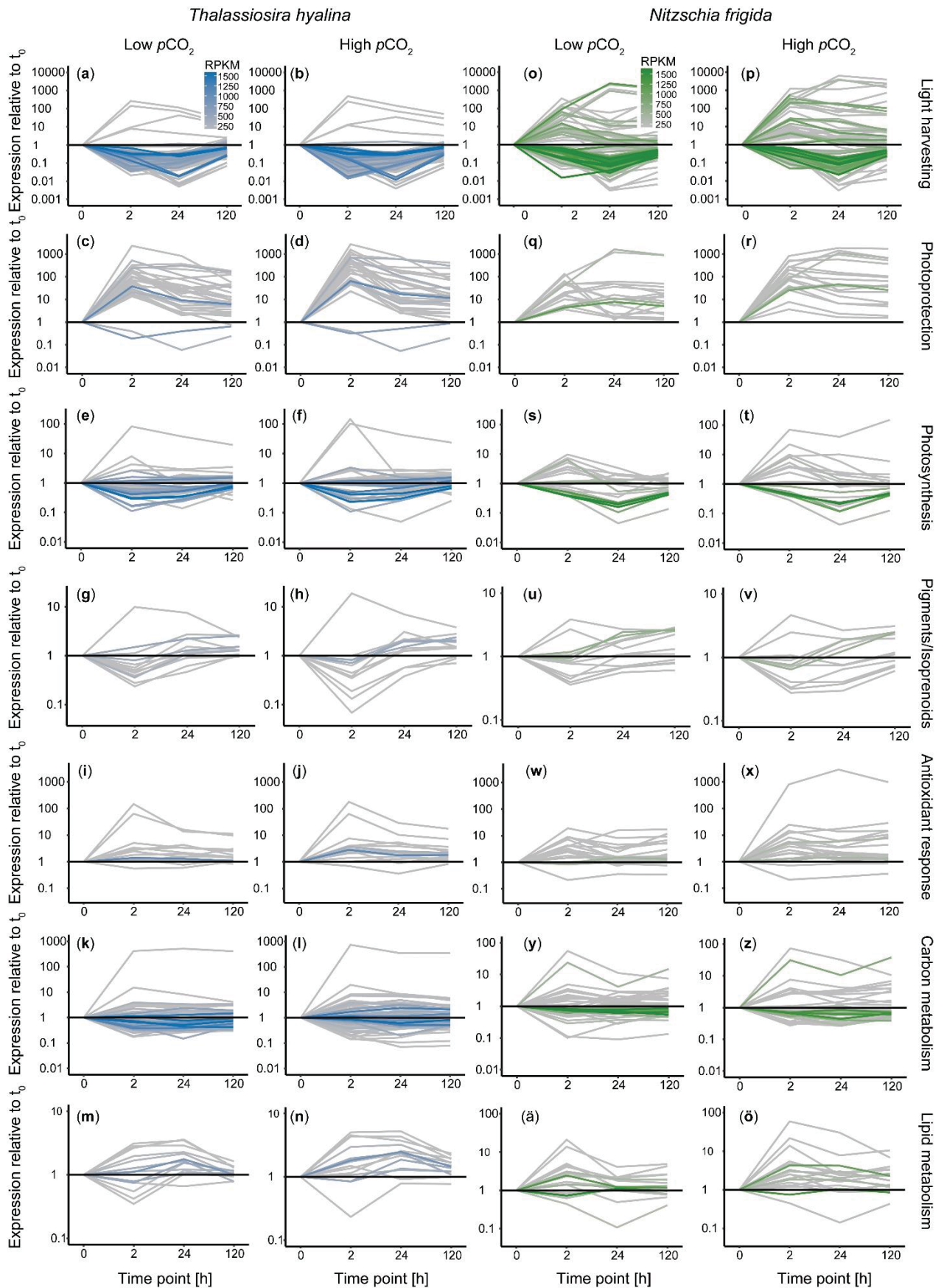
Fig. 1:

Fig. 2:

Fig. 3:

Thalassiosira hyalina .... _Nitzschia frigida_

Low pCO$_2$ · High pCO$_2$ · Low pCO$_2$ · High pCO$_2$

Light harvesting · Photoprotection · Photosynthesis · Pigments/Isoprenoids · Antioxidant response · Carbon metabolism · Lipid metabolism
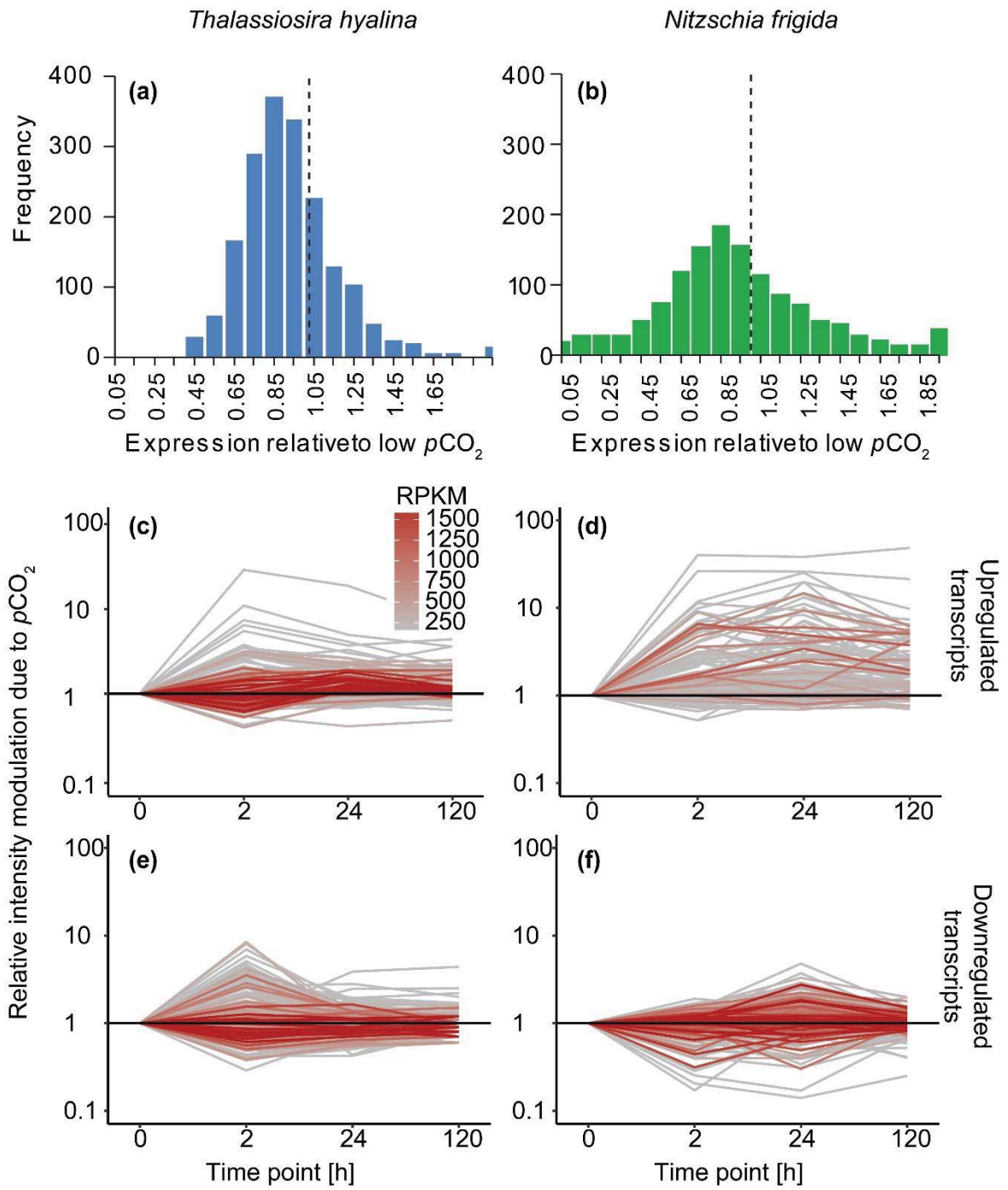
Expression relative to t_0

Time point [h]

Fig. 4:

Supplementary material, Fig. S1: